NANO · MICRO small
www.small-journal.com

Protein Nanopore Membranes Prepared by a Simple Langmuir–Schaefer Approach

Magnus S. Schwieters, Maria Mathieu-Gaedke, Michael Westphal, Raphael Dalpke, Maxim Dirksen, Daizong Qi, Marco Grull, Thomas Bick, Stephanie Taßler, Daniel F. Sauer, Mischa Bonn, Petra Wendler, Thomas Hellweg, André Beyer, Armin Gölzhäuser, Ulrich Schwaneberg, Ulrich Glebe, and Alexander Böker**

Filtration through membranes with nanopores is typically associated with high transmembrane pressures and high energy consumption. This problem can be addressed by reducing the respective membrane thickness. Here, a simple procedure is described to prepare ultrathin membranes based on protein nanopores, which exhibit excellent water permeance, two orders of magnitude superior to comparable, industrially applied membranes. Furthermore, incorporation of either closed or open protein nanopores allows tailoring the membrane's ion permeability. To form such membranes, the transmembrane protein ferric hydroxamate uptake protein component A (FhuA) or its open-pore variant are assembled at the air–water interface of a Langmuir trough, compressed to a dense film, crosslinked by glutaraldehyde, and transferred to various support materials. This approach allows to prepare monolayer or multilayer membranes with a very high density of protein nanopores. Freestanding membranes covering holes up to 5 µm in diameter are visualized by atomic force microscopy (AFM), helium ion microscopy, and transmission electron microscopy. AFM PeakForce quantitative nanomechanical property mapping (PeakForce QNM) demonstrates remarkable mechanical stability and elastic properties of freestanding monolayer membranes with a thickness of only 5 nm. The new protein membrane can pave the way to energy-efficient nanofiltration.

1. Introduction

Membranes for the separation of (nano-) particles and even small molecules from a solution are used in various applications, including wastewater treatment,[1] water desalination,[2] and biomedical hemodialysis.[3] Nowadays, most such membranes are made of polymers by phase inversion, interfacial polymerization, or a combination of both.[4] By phase inversion, integral asymmetric membranes with pores of rather random size and orientation are formed, limiting both selectivity and permeability.[3] By interfacial polymerization, composite membranes with a thin and dense top layer are prepared. Although optimizing such membranes is well-advanced, transport across this dense selective layer requires high transmembrane pressures and high energy consumption. Substantial improvement of membrane processes regarding energy efficiency and separation precision thus

M. S. Schwieters, M. Mathieu-Gaedke, U. Glebe, A. Böker
Fraunhofer Institute for Applied Polymer Research IAP
Geiselbergstr. 69, 14476 Potsdam-Golm, Germany
E-mail: ulrich.glebe@iap.fraunhofer.de;
alexander.boeker@iap.fraunhofer.de

M. S. Schwieters
Polymer Engineering/Polymer Physics
Berlin Institute of Technology (TU Berlin)
Ernst-Reuter-Platz 1, 10587 Berlin, Germany

M. Mathieu-Gaedke, A. Böker
Chair of Polymer Materials and Polymer Technologies
Institute of Chemistry
University of Potsdam
Karl-Liebknecht-Str. 24–25, 14476 Potsdam-Golm, Germany

The ORCID identification number(s) for the author(s) of this article can be found under https://doi.org/10.1002/smll.202102975.

DOI: 10.1002/smll.202102975

M. Westphal, R. Dalpke, A. Beyer, A. Gölzhäuser
Physics of Supramolecular Systems and Surfaces
Faculty of Physics
Bielefeld University
Universitätsstr. 25, 33615 Bielefeld, Germany

M. Dirksen, T. Hellweg
Department of Physical and Biophysical Chemistry
Faculty of Chemistry
Bielefeld University
Universitätsstr. 25, 33615 Bielefeld, Germany

D. Qi, M. Bonn
Max Planck Institute for Polymer Research
Ackermannweg 10, 55128 Mainz, Germany

M. Grull, D. F. Sauer, U. Schwaneberg
Institute of Biotechnology
RWTH Aachen University
Worringer Weg 3, 52074 Aachen, Germany

T. Bick, P. Wendler
Department of Biochemistry
University of Potsdam
Karl-Liebknecht-Str. 24–25, 14476 Potsdam-Golm, Germany

requires fundamentally new concepts. Ideally, a membrane would be ultrathin, yet stable in a pressure-driven filtration process, and have densely packed, monodisperse pores aligned vertically to the membrane plane.[3] Promising approaches toward such membranes include graphene-[5] and carbon-nanotube-based[6] membranes, as well as ultrathin carbon nanomembranes prepared by crosslinking of self-assembled monolayers, e.g., from terphenylthiol molecules.[7,8] Furthermore, self-assembled block-copolymer membranes with nearly monodisperse nanometer-sized pores in a thin selective layer and strategies for tailoring the pore size and functionality have been introduced.[9] Another group of promising approaches may be found in bioinspired membranes.

Biological membranes, on a cellular scale, fulfill many of the aforementioned criteria. Biological membranes separate cells or cell components and mainly consist of a dense phospholipid bilayer that is less than 10 nm thick. The phospholipid bilayer incorporates membrane proteins, which enable signal transmission and selective transport of molecules across the membrane. Membrane proteins connecting both sides of the membrane are referred to as transmembrane proteins (TPs), and some TPs form a nanopore.[10] Since such TPs are truly monodisperse pores and their large-scale biotechnological production and modification have seen significant progress, TPs can be considered as functional building blocks for the engineering of new biohybrid membranes.[10–12] In the past, TPs have been incorporated and studied in lipid or block copolymer bilayers, which mimic the natural phospholipid bilayer of biological membranes.[13,14] Those TP-loaded bilayers have been either vesicles,[15–18] then referred to as lipo- or polymersomes, or planar nanosheets.[18,19] Vesicle-spreading or layering of nanosheets on top of membrane supports has allowed to prepare highly permeable, planar membranes with TPs acting as monodisperse nanopores.[16,20,21] However, the incorporation of TPs into lipid or block copolymer bilayers solely relies on noncovalent interactions, limiting the membrane stability. Furthermore, homogeneous defect-free vesicle spreading is highly challenging.[22,23] Alternatively, the incorporation of whole liposomes with inserted TPs in a membrane has been investigated.[24] Such membranes were thicker and more stable, but less energy-efficient as compared to ultrathin approaches. It should also be mentioned that membrane preparation based on lipid or block copolymer bilayers is solely suited for TPs and, so far, the incorporation of other interesting biological nanopores, such as virus-like particles derived from tobacco mosaic virus (TMV),[25] into stable membranes has required rather cumbersome procedures.[26,27]

To bypass these limitations, we pursue different strategies of membrane fabrication that provide covalent stabilization and dense arrangement of protein nanopores. Previously, we crosslinked ferritin–polymer conjugates to ultrathin membranes and formed nanopores by denaturation of the protein.[28–32] Using naturally pore-forming TPs instead of ferritin, we synthesized TP-polymer conjugates,[33] which were transformed into stable membranes by assembly at Pickering emulsion interfaces and subsequent UV crosslinking of the polymer chains.[34] Here, we present a straightforward method for the integration of functional TPs into planar ultrathin membranes. This strategy is based on the Langmuir technique and the homobifunctional crosslinker glutaraldehyde, being an efficient protein crosslinker and known not to impact the protein conformation in many cases.[35–37] For demonstration, two variants of the largest monomeric β-barrel TP ferric hydroxamate uptake protein component A (FhuA) were used: the naturally occurring FhuA wild type (FhuA WT) with an almost closed pore and the engineered FhuA ΔCVF^{tev} variant with an open pore (**Figure 1**a). Both variants have an elliptical cross-section of 3.9–4.6 nm and a height of 6.9 nm. The FhuA ΔCVF^{tev} pore has an inner diameter of (2.6 ± 0.6) nm,[38] yet engineering of FhuA variants with larger pore diameters is possible.[38,39] FhuA WT and FhuA ΔCVF^{tev} have 37 and 28 lysine residues, respectively, distributed over their lateral surface and allowing for dense chemical crosslinking with glutaraldehyde. Additionally, FhuA ΔCVF^{tev} has an accessible cysteine residue inside the open pore, which enables chemical modification with thiol-reactive groups. FhuA is an amphiphilic protein characterized by a hydrophobic transmembrane region and a hydrophilic loop region. Due to its pronounced amphiphilicity, FhuA has a strong tendency to assemble at interfaces, as we have demonstrated before with tensiometry measurements.[34] In this study, FhuA molecules were spread at the air–water interface of a Langmuir trough (Figure 1b(i)). Upon compression with the two movable barriers of the Langmuir trough, a dense 2D film was formed and stabilized by glutaraldehyde crosslinking. Single or multiple layers of crosslinked FhuA membranes were transferred to various substrate materials using the Langmuir–Schaefer method (Figure 1b(ii)).[40] FhuA membranes covered holes in substrates without tearing and elastically stretched when loaded with a point force in AFM measurements, which demonstrates great mechanical stability. Membranes were prepared from either FhuA WT or FhuA ΔCVF^{tev} that naturally form almost closed or completely open pores, respectively (Figure 1c). Even membranes with almost closed FhuA pores showed outstanding water permeance, two orders of magnitude superior to state-of-the-art thin-film composite nanofiltration membranes. This is attributed to their low thickness of only a few molecular layers. Moreover, membranes prepared using the open pore variant showed higher ion permeability over those prepared using the closed pore variant (Figure 1d).

2. Results and Discussion

2.1. Membrane Preparation

To prepare FhuA membranes, 0.32 nmol of FhuA WT or FhuA ΔCVF^{tev} in MPD buffer (Figure S1, Supporting Information) were spread to the air–water interface of the Langmuir trough. This is less FhuA than needed to fully cover the initial trough area (area of the air–water interface between the Langmuir trough barriers) and ensures that the adsorbed FhuA film rather consists of one than multiple molecular layers (Figure S2, Supporting Information). FhuA adsorption

S. Taßler
Synchrotron SOLEIL
L'Orme des Merisiers
BP48, Gif-Sur-Yvette, Saint-Aubin 91192, France
U. Schwaneberg
DWI – Leibniz Institute for Interactive Materials e.V.
Forckenbeckstr. 50, 52056 Aachen, Germany

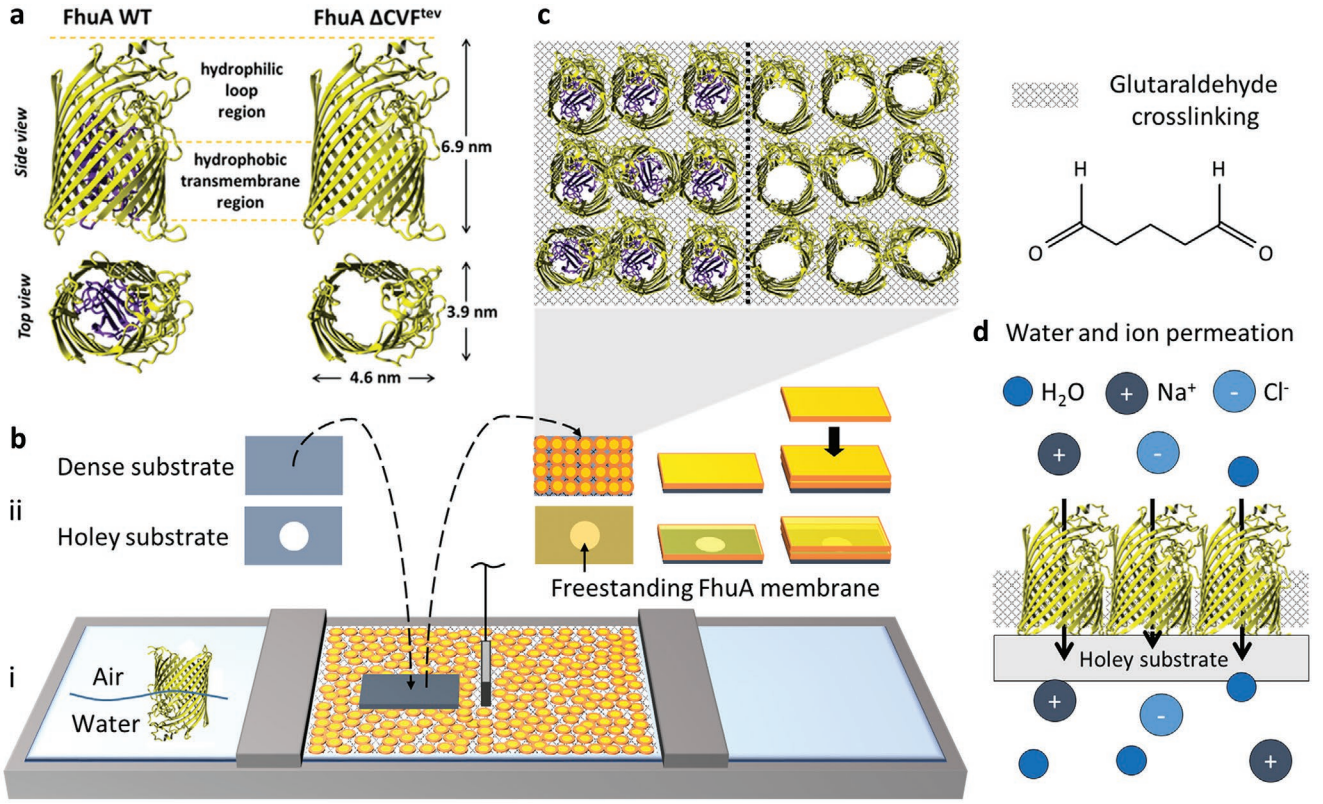

Figure 1. Crosslinked 2D membrane sheets of transmembrane protein FhuA. a) Two variants of the ß-barrel protein FhuA were used. In FhuA WT, a cork domain blocks most of the pore interior while this cork domain was biotechnologically removed to form the open pore variant FhuA ΔCVF^{tev}. Both FhuA variants have identical dimensions and are characterized by a hydrophilic loop region in the upper part of the protein and a hydrophobic transmembrane region in the lower part of the protein. b) Langmuir technique was applied to form ultralarge 2D FhuA membrane sheets. (i) Due to their amphiphilicity, FhuA molecules occupy a largely upright orientation when spread to the air–water interface. (ii) When densely compressed between the barriers of the Langmuir trough and crosslinked with glutaraldehyde, FhuA membrane sheets can be layered on top of substrates by repeated horizontal dipping. By using holey substrates, freestanding FhuA membranes can be fabricated. c) Schematic top view of membranes made of FhuA WT (left) or FhuA ΔCVF^{tev} (right) and structural formula of glutaraldehyde. d) FhuA membranes were characterized in terms of water and ion permeation.

was monitored as a function of surface pressure over time (**Figure 2**a(i)), showing an initial rise in surface pressure until asymptotically approaching an equilibrium between 2 and 2.5 mN m^{-1} after 2 h. Upon reducing the trough area by barrier compression, the surface pressure increased almost linearly (Figure 2a(ii)). This indicates an increasing surface concentration and thus the formation of a denser FhuA film at the air–water interface. To our knowledge, investigations of Langmuir films of solely TPs have previously only been published for bestrophin-1, when studying molecular mechanisms underlying specific pathologies linked to this protein.[41,42] To observe FhuA film formation on the microscale, Brewster angle microscopy (BAM) was applied. BAM showed a homogenous FhuA film for surface pressures below 30 mN m^{-1}, while elongated cracks were visible at higher surface pressures (Figure 2b; Figure S3, Supporting Information). To prevent cracks but form a densely packed FhuA membrane, crosslinking with glutaraldehyde was performed at a surface pressure of 25 mN m^{-1}. Injection of glutaraldehyde into the buffer subphase was carried out reaching a final concentration of 0.5 vol% and is visible as a small irritation in the compression curve at a trough area of 112 cm^2 (marked with an arrow in Figure 2a(ii),(iii)). Efficient FhuA crosslinking at this glutaraldehyde concentration in solution was verified by SDS-PAGE (Figure S1, Supporting Information). The plateau in the compression curve indicates that keeping the surface pressure constant requires further reduction of the trough area (Figure 2a(ii)). However, the kink in the trough area–time curve (Figure 2a(iii)) illustrates that shortly after the injection of glutaraldehyde (marked with an arrow), the membrane area stabilizes at a trough area of around 100 cm^2. A comparison of trough area reduction over time at a surface pressure of 25 mN m^{-1} with and without the injection of glutaraldehyde is shown in Figure S4 of the Supporting Information. Without the addition of glutaraldehyde, the trough area reduces at high rates, which is attributed to FhuA molecules desorbing from the surface into the subphase due to the high surface pressure.[43,44] When glutaraldehyde is added, however, the trough area soon reduces at significantly lower rates, pointing to covalent bonds forming between the lysine residues of adsorbed FhuA molecules and consequent stabilization of the FhuA film at the air–water interface. To investigate the alignment of FhuA molecules at the air–water interface before and after crosslinking, sum-frequency generation (SFG) spectroscopy was used. SFG is a surface-sensitive vibrational spectroscopy technique, which provides the vibrational spectrum of the interfacial region for which symmetry is broken. In this approach, visible and infrared laser pulses impinge upon the surface, and SFG light, at a frequency given by the sum of the visible and infrared

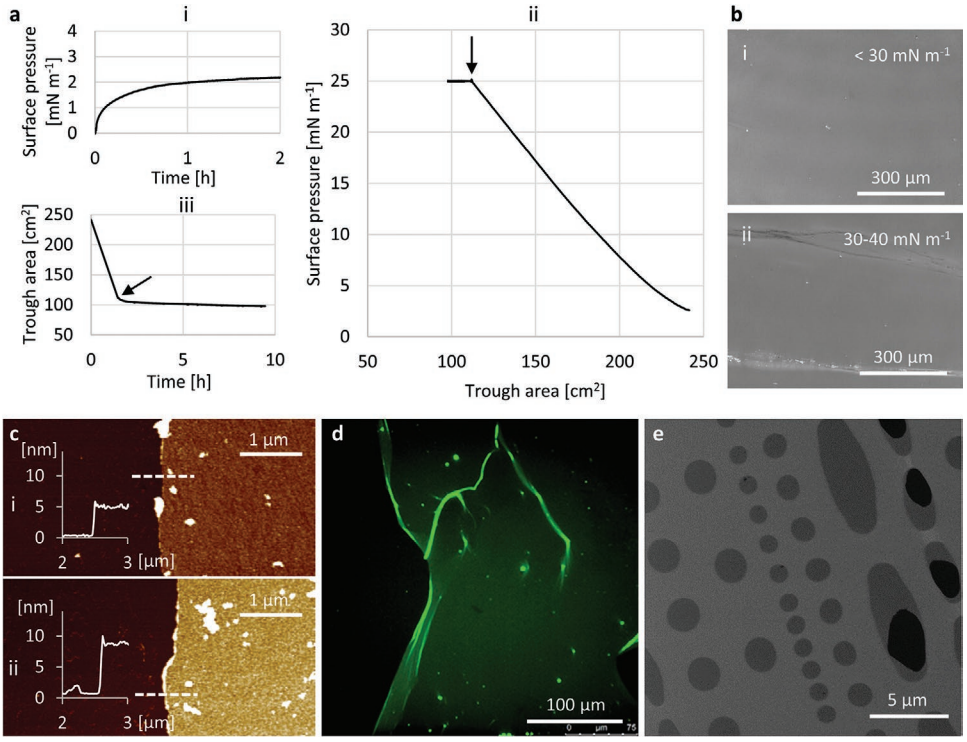

Figure 2. FhuA membranes at the air–water interface and transferred to substrates. a) Representative set of Langmuir (i) adsorption, (ii) compression, and (iii) trough area-time curves measured during membrane fabrication from 0.32 nmol FhuA WT spread on top of phosphate buffer (pH 7.4). In (ii) and (iii), the injection of glutaraldehyde is marked with an arrow. b) Corresponding BAM imaging showed (i) a homogenous FhuA membrane up to surface pressures of 30 mN m^{-1}. (ii) At surface pressures exceeding 30 mN m^{-1}, extended cracks appeared in the FhuA membrane. c) AFM images of (i) one or (ii) two FhuA membrane sheets layered on top of a silicon substrate (left half scratched away with a syringe tip). The height profiles belong to the dashed lines in the images and indicate membrane thicknesses of (i) 5 and (ii) 9 nm. d) Confocal fluorescence microscopy image of a single FhuA ΔCVF^{tev} membrane sheet on top of a silicon substrate labeled with a fluorescence marker. e) HIM image of a FhuA WT membrane freestandingly covering holes (dark gray) in the structured carbon film of a TEM grid (light gray). The black areas show defects in the membrane.

frequencies, is generated when the infrared is resonant with interfacial vibrations—in this case the protein amide mode.[45] SFG measurements demonstrated upright and collective orientation of FhuA molecules at the air–water interface, and crosslinking did not impact this constitution (Figure S5, Supporting Information). Generally, FhuA WT and FhuA ΔCVF^{tev} samples showed similar adsorption behavior, and membranes of both variants were prepared in an analogous manner. Measurements corresponding to the membrane formation with FhuA ΔCVF^{tev} are shown in Figure S6 of the Supporting Information. After 8 h of crosslinking, the FhuA WT and the FhuA ΔCVF^{tev} membranes covered areas of 95.7 and 97.4 cm^2, respectively.

Combining knowledge from SFG measurements (upright FhuA orientation at the air–water interface, Figure S5, Supporting Information) with an approximation of the area occupied by uprightly oriented FhuA molecules as derived from its crystal structure (Figure S2, Supporting Information), the maximum packing density of FhuA molecules in FhuA membranes was estimated. If all spread FhuA molecules (0.32 nmol) arranged in upright fashion at the air–water interface (neglecting desorption into the subphase), they would cover an area of about 78 cm^2 (Figure S2, Supporting Information). Relating this area to the final FhuA membrane area of about 96 cm^2, results in a maximum packing density of 80%, the other 20 % being interstitial space between the FhuA molecules. However, the interstitial space in this upper bound scenario is at least partly filled with glutaraldehyde. Therefore, the interstitial space may contribute to water flux and ion permeability through FhuA membranes, but is presumably blocked for transport of larger molecules or particles during filtration experiments.

2.2. Transfer to Supports

Crosslinked FhuA membranes were transferred from the air–water interface to various substrates by the Langmuir–Schaefer method.[40] By single or multiple dipping, mono- or multilayers could be transferred. FhuA membranes consisting of one or two layers showed a thickness of 5 and 10 nm, respectively, when transferred to silicon substrates and analyzed by atomic force microscopy (AFM) (Figure 2c). Those values were confirmed by specular X-ray reflectivity measurements on mono- and double-layer FhuA membranes (Figure S7, Supporting Information). Considering possible drying effects, the measured monolayer thickness of 5 nm matches the theoretical dimensions of a single FhuA molecule (Figure 1a). This indicates successful preparation of 2D FhuA membrane sheets. However, performing grazing-incidence small-angle X-ray scattering on FhuA membranes transferred to silicon substrates, no diffraction pattern indicating a defined repeating distance was observed (Figure S8, Supporting Information). Hence, the

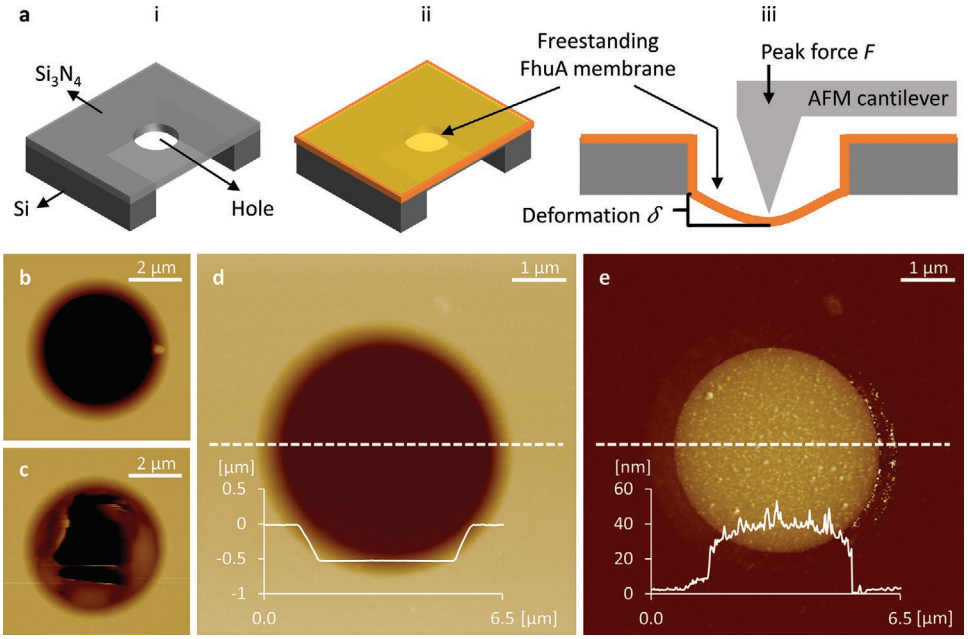

Figure 3. AFM measurements on FhuA monolayer membranes. a) Schematic illustration of a silicon nitride membrane window with a single hole in its center when (i) not covered and (ii) covered with a FhuA membrane. (iii) Cross-section of the FhuA membrane-coated silicon nitride membrane window during AFM imaging in PeakForce QNM mode,[47] in which the cantilever deforms the freestanding membrane until a set peak force is reached. b–d) AFM height images of the hole in the silicon nitride membrane window when (b) the hole was not covered with a FhuA membrane, (c) the hole was covered with a ruptured FhuA ΔCVF^{tev} membrane, and (d) the hole was covered with a single, intact FhuA ΔCVF^{tev} membrane layer. e) AFM deformation image showing the membrane deformation at the peak force of 2 nN. Height and deformation images in (d) and (e) were acquired simultaneously, and all images were measured in water. The height and deformation profiles in (d) and (e) belong to the dashed lines in the images, respectively.

proteins in the thin films do not have a crystalline-like ordering. To test the structural integrity of membrane-incorporated FhuA, six FhuA ΔCVF^{tev} membrane sheets were layered on top of a cuvette glass (Figure S9, Supporting Information) and analyzed using circular dichroism (CD) spectroscopy. The corresponding CD spectrum resembles the CD spectrum of FhuA ΔCVF^{tev} in MPD buffer (Figure S10, Supporting Information), indicating an intact secondary structure of FhuA as part of the transferred and dried membrane. Evidence of intact tertiary protein structure was obtained indirectly. The free-cysteine residue inside the open pore of FhuA ΔCVF^{tev} could be successfully labeled with the thiol-reactive fluorescence marker ThioGlo1, even when FhuA ΔCVF^{tev} was already incorporated in a membrane (Figure 2d). This implies the presence and accessibility of intact FhuA pores in crosslinked FhuA ΔCVF^{tev} membranes and thus intact tertiary FhuA structure. The fluorescence microscopy image in Figure 2d also demonstrates the vast lateral expansion of a single FhuA membrane sheet as compared to its shallow thickness. To be applied in a membrane process, FhuA membranes are required to freestandingly cover microporous substrate materials. FhuA membranes covered elliptical holes in transmission electron microscopy (TEM) grids with dimensions of up to 2 µm × 8 µm without tearing, as shown in the helium ion microscopy (HIM) image in Figure 2e and confirmed by AFM analysis (Figure S11, Supporting Information). High-resolution TEM was challenging as FhuA membranes rupture when exposed to high-intensity electron beams. The TEM image of a rupturing FhuA ΔCVF^{tev} membrane stained with uranyl acetate (UA) in Figure S12 of the Supporting Information shows a homogenous nanoscale pattern that is very similar to that of UA stained carbon films. This limits the interpretation of the pattern regarding structural features of the FhuA ΔCVF^{tev} membrane. Although high-resolution cryo-TEM imaging showed FhuA membranes to be very homogenous (Figure S13, Supporting Information), it lacks contrast to reveal information about the presence of FhuA pores.

In preparation of water permeation and ion conductivity measurements, single FhuA membrane sheets were transferred to silicon nitride membrane windows with a hole (Ø 5 µm) in its center (**Figure 3**a(i),(ii)). Coated silicon nitride membrane windows were analyzed using the AFM PeakForce quantitative nanomechanical property mapping (PeakForce QNM) mode in liquid,[46] in which the AFM cantilever is moved toward the sample until a certain peak force is reached (here 2 nN) (Figure 3a(iii)). In PeakForce QNM, with each cantilever-sample interaction a so-called force–distance curve is measured. Software-controlled analysis of such curves allows to simultaneously acquire both, the typical AFM height image and an AFM deformation image, showing the local sample deformation upon cantilever loading at the peak force.[46] Here, AFM height images clearly allow discriminating the open hole in a silicon nitride membrane from holes covered with a defect or intact FhuA monolayer membrane (Figure 3b–d). The height profile of the intact FhuA ΔCVF^{tev} membrane in Figure 3d indicates that the membrane recedes about 500 nm into the hole. This is exactly the thickness of the silicon nitride membrane and similar behavior was reported by Mueggenburg et al. for monolayer membranes of close-packed gold nanoparticles covering a holey silicon nitride membrane with a thickness of 100 nm.[47] The AFM deformation image belonging

to the height image of the intact FhuA ΔCVF^{tev} membrane (Figure 3d) is shown in Figure 3e. The deformation profile confirms that the freestanding FhuA ΔCVF^{tev} membrane elastically stretched up to 40 nm when loaded with the peak force of 2 nN. While repeated imaging did not change the results, this demonstrates enormous mechanical stability of FhuA membranes made out of a single protein layer. Additionally, two more FhuA ΔCVF^{tev} membranes were investigated, discreetly increasing the peak force to 2, 5, and 10 nN (Figure S14, Supporting Information). As expected, higher peak forces resulted in higher membrane elongation of maximum 250 nm, when loaded with the peak force of 10 nN. At peak forces higher than 10 nN, the samples were uncontrollably moved by the cantilever–sample interaction, restricting determination of a stability limit of FhuA membranes for this method. Studying their gold nanoparticle membranes, Mueggenburg et al. deduced a mathematical model to estimate the Young's modulus of homogenous membranes covering a hole and loaded with a point force in central position.[47–49] Filling this model with data from the PeakForce QNM measurements presented in Figure 3, results in a Young's modulus of the FhuA ΔCVF^{tev} membrane of 37 GPa (for calculation see the Experimental Section). Values for the Young's modulus of the two other FhuA ΔCVF^{tev} membranes tested with varying peak forces range between 1.5 and 11.5 GPa (Figure S14, Supporting Information). Interestingly, these values closely resemble the range of Young's moduli (3–39 GPa) stated by Mueggenburg et al. when measuring 19 gold nanoparticle monolayer membranes in their study. This suggests similar elastic properties of the two freestanding monolayer membranes when probed by AFM, even though the bulk material gold is assumed to be significantly stiffer than proteins.

2.3. Water Permeance

The water permeance of FhuA WT membranes was measured with a mass loss method.[50] First, the single hole (Ø 5 µm) in a silicon nitride membrane window was coated with one, two or five FhuA WT membrane layers (Figure 3). The preparation of one FhuA WT membrane at the air–water interface of the Langmuir trough was sufficient to coat multiple silicon nitride membrane windows with multiple FhuA WT membrane layers (Figures S15 and S16, Supporting Information). An HIM image of a freestanding FhuA WT membrane on top of the 5 µm hole is shown in Figure S17 of the Supporting Information. Next, the coated chip was glued to a container cap, which in return was screwed on top of a container filled with 400 µL of water (**Figure 4**a,b). The only way for water to evade the container was to permeate the FhuA WT membrane on top of the hole. The driving force of this permeation process is the difference in water vapor pressure from the container inside to the outside, which was kept constant during the experiment (Figure 4a). The permeance was calculated by relating the mass of permeated water to the duration of the experiment, the water vapor pressure difference, and the FhuA WT membrane area. To distinguish intact from defect FhuA WT membranes, samples were analyzed by AFM and HIM after the experiment (Figure S18, Supporting Information). All single-layer FhuA WT membranes broke during the experiment. Several FhuA WT membranes consisting of two or five layers remained stable, showing average permeances of 3.87×10^4 mol Pa^{-1} m^{-2} s^{-1}. Compared to reference measurements in which the hole remained uncovered, FhuA WT membranes reduced water evaporation from the cup by a factor of 6.5. Permeances of defect FhuA WT membranes lay between the permeances measured for references and intact FhuA WT membranes (Figure 4c). The measured water permeance of FhuA WT membranes falls within the range of water permeances reported for other biomimetic membranes with nanopores (FhuA 1.11×10^4 mol Pa^{-1} m^{-2} s^{-1};[20] TMV 10.76×10^4 mol Pa^{-1} m^{-2} s^{-1};[27] Aquaporin Z 0.92×10^4 mol Pa^{-1} m^{-2} s^{-1} and 0.05×10^4 mol Pa^{-1} m^{-2} s^{-1}[15,16]) and ultrathin carbon nanomembranes (1.1×10^4 mol Pa^{-1} m^{-2} s^{-1},[7] tested in the same set-up). FhuA WT membranes thus show more than 150 times greater water permeance than the polyamide thin-film composite membrane FilmTec NF270 (0.023×10^4 mol Pa^{-1} m^{-2} s^{-1}, MWCO 400 Da, DuPont de Nemours Inc., USA), which performed best in a water permeance comparison among eight commercial membranes in the sub-nanometer to few-nanometer separation range in 2020.[20] Here, FhuA WT membranes (with "closed" pores) were investigated showing extremely high permeances. It should be pointed out that the pore of FhuA WT is blocked by a cork domain, but not closed in a sealed way. In fact, the cork domain is known to allow water transport.[51] Additionally, considering the FhuA membrane packing density of maximum 80% (as estimated above), water permeation will very likely also occur through the interstitial spaces between the crosslinked FhuA molecules. In conclusion, the presented mass loss method nicely highlights the overall very high water permeance of FhuA membranes.

2.4. Ion Permeability

Black lipid membrane experiments by Killmann et al. have demonstrated that open-pore variants of FhuA form an ion-permeable, water-filled diffusion pore. The experiments have further suggested that the cork domain in FhuA WT significantly reduces FhuA's ion permeability by about 80% (factor 6), so that only minor current fluctuations were detected.[13] To test if the different ion permeabilities transfer to membranes prepared from FhuA WT and FhuA ΔCVF^{tev}, conductance measurements were performed as follows: Five FhuA membrane sheets were layered on top of a silicon nitride membrane chip having a single hole with a diameter of 1 µm. The resulting FhuA membrane thickness of a little more than 20 nm was verified by AFM before the experiment to only include FhuA WT and FhuA ΔCVF^{tev} membranes of identical thickness (Figure S19, Supporting Information). As a reference, silicon nitride membrane windows without FhuA membranes on top were used. The samples were mounted between two parts of a microfluidic measurement chamber filled with a phosphate buffer. Two electrodes connected to a voltage source were immersed into the buffer on both sides of the membrane, and the resulting current was measured while successively increasing the voltage (Figure 4d). After the experiment, the integrity of FhuA membranes on top of the hole was verified by AFM (Figure S19, Supporting Information). The current–voltage curves (*I–V* curves)

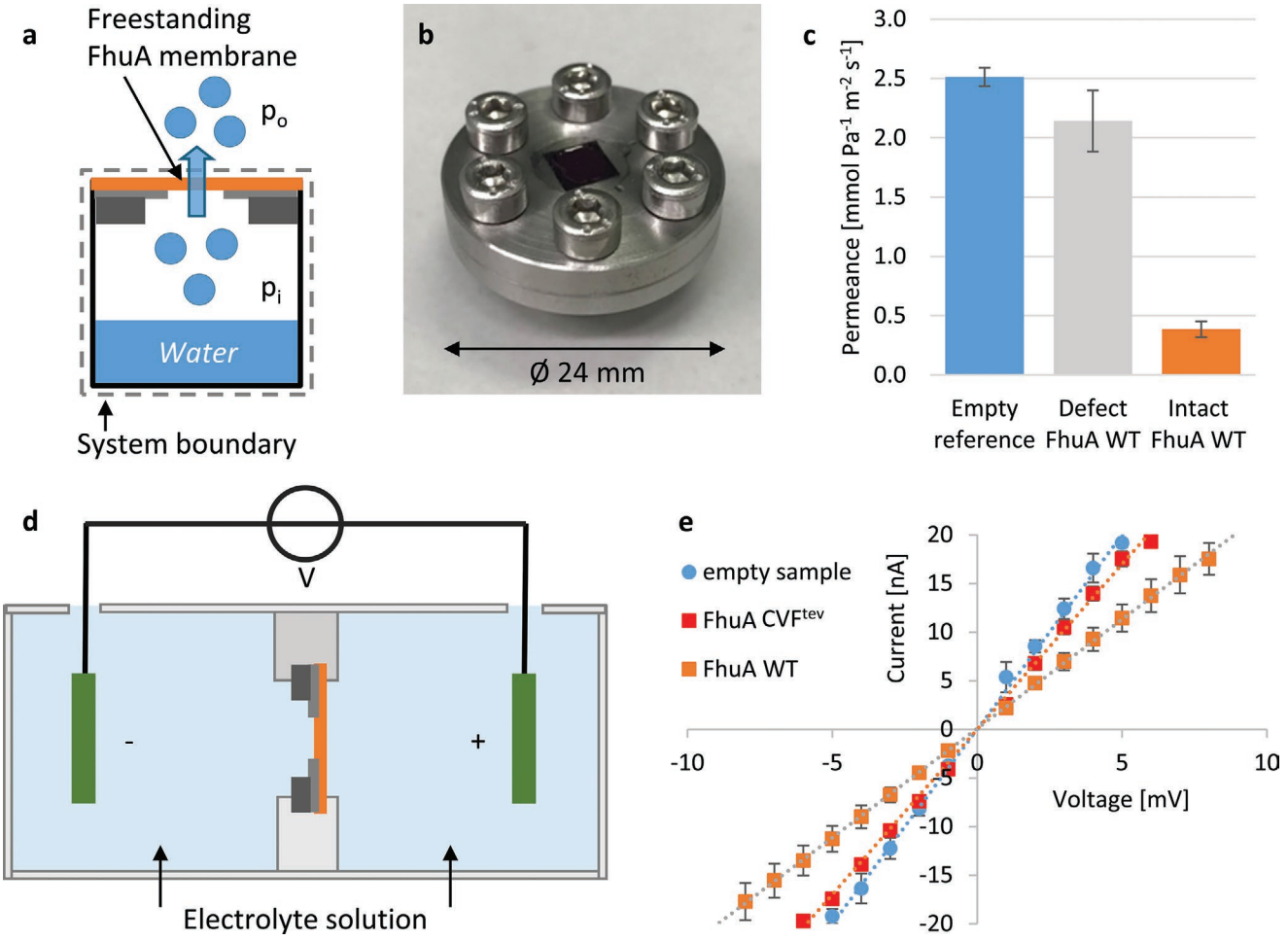

Figure 4. Water and ion permeation through FhuA membranes. a) Schematic illustration of the water-filled container covered with a silicon nitride membrane window as used to measure the water permeance of FhuA WT membranes. Driven by the water vapor pressure difference from the cup inside to the outside (p_i–p_0), the only way for water to escape the cup was to permeate the FhuA WT membrane. b) Photograph of the cup illustrated in (a). c) The water permeance of FhuA WT membranes was 3.87×10^4 mol Pa^{-1} m^{-2} s^{-1} (empty reference 25.13×10^4 mol Pa^{-1} m^{-2} s^{-1}). Error bars indicate the standard error of mean of at least three samples. d) Schematic illustration of the experimental set up used to measure the ion permeability of FhuA membranes. The only way for ions to diffuse between the electrodes was to permeate the FhuA membrane on top of the hole in the silicon nitride membrane window. e) Current–voltage curves measured in phosphate buffer (10×10^{-3} M NaCl, 10×10^{-3} M sodium phosphate (NaPi), pH = 7). The constant slopes correspond to constant conductances between the electrodes of 4.0 mS (empty reference), 3.4 mS (FhuA ΔCVF^{tev} membrane, five layers), and 2.3 mS (FhuA WT membrane, five layers). Error bars indicate the standard error of mean of at least three samples.

of each three references, FhuA WT and FhuA ΔCVF^{tev} membranes were measured and the averaged results are shown in Figure 4e. The measurement set-up allowed to register currents up to ±20 nA. Within this range, the *I*–*V* curves for the references as well as for FhuA WT and FhuA ΔCVF^{tev} membranes are linear. The constant slopes of the *I*–*V* curves correspond to constant conductances of 4.0 mS when the hole was not covered with a membrane and 3.4 or 2.3 mS when a FhuA ΔCVF^{tev} or FhuA WT membrane covered the hole, respectively. Compared to the reference, FhuA ΔCVF^{tev} or FhuA WT membranes are permeable for 85% or 58% of the ions. These findings indicate that the different ion permeabilities of FhuA WT and FhuA ΔCVF^{tev} demonstrated in black lipid membrane experiments indeed transfer to FhuA membranes made from each variant to some extent. This strongly suggests the incorporation of structurally intact FhuA pores into a 2D membrane. However, even FhuA WT membranes showed rather high ion conductivity, which was not 80% lower (as reported from the FhuA variants tested in black lipid membranes) but only 30% lower than that of FhuA ΔCVF^{tev} membranes. While such direct comparison has limited meaning, because black-lipid membrane experiments were done using a different buffer and voltage, influence of ion permeation through the interstitial space between the FhuA molecules is very likely to have contributed to ion permeation of both FhuA WT and FhuA ΔCVF^{tev} membranes as well. Nonetheless, FhuA membranes were layered to increase the mechanical stability of the membrane and—from a statistical point of view—it is thus likely that most ions passed at least one channel when permeating the multilayer membranes.

Layering FhuA membranes may also help to decrease negative influence of membrane defects and interstitial spaces when comparing the membranes' size selectivity. First attempts toward FhuA membrane transfer to scalable ceramic

membrane supports, and subsequent filtration experiments analyzing the size selectivity showed BSA rejection of up to 80% (Figures S20 and S21, Supporting Information). However, BSA (hydrodynamic radius ≈3.5 nm)[52] should pass through neither FhuA WT nor FhuA ΔCVF^{tev} membranes at all, and the BSA flux was assigned to incomplete coating of the membrane supports with FhuA membranes. Improved, automated FhuA membrane transfer to membrane supports is currently being investigated. Once dense, reproducible coating is implemented, a detailed study of the different size selectivity expected between the open pore and closed pore FhuA membranes will follow.

3. Conclusion

Here, we introduced a new method for the fabrication of ultrathin, yet mechanically stable membranes incorporating the TP FhuA, which naturally forms a defined nanopore. Due to their low thickness and the extremely high density of collectively aligned proteins inferred in this study, such membranes have very high water permeance compared to conventional nanofiltration membranes. Membranes made of two different FhuA variants mirrored the molecular properties of each variant, here demonstrated with respect to ion permeability. Given intensive research on imprinting functionalities to protein nanopores,[11,53–55] our membrane has potential to serve as a platform technology that allows tailoring membranes according to individual process requirements. Membrane fabrication uses the well-studied Langmuir technique and a common protein crosslinker, which ensures good scalability with a view to future applications.

4. Experimental Section

Buffer: In this study, MPD buffer is defined as a buffer containing 7.5×10^{-3} M sodium hydrogen phosphate (Na_2HPO_4), 2.5×10^{-3} M sodium dihydrogen phosphate (NaH_2PO_4), and 50×10^{-3} M 2-methyl-2,4-pentanediol (MPD). MPD is used as a stabilizing agent for FhuA variants in this study.[56,57] Phosphate buffer is defined as a buffer containing 7.5×10^{-3} M sodium hydrogen phosphate (Na_2HPO_4) and 2.5×10^{-3} M sodium dihydrogen phosphate (NaH_2PO_4). Buffers were made using Millipore pure water with a resistivity of 18.2 MΩ cm.

FhuA Expression and Refolding: Engineering, expression and extraction of the FhuA variants used in this study were performed according to previously published procedures.[58] The lyophilized powder of the respective FhuA variant (containing ≈66 wt% SDS) was dissolved in MPD buffer and passed through a sterile 0.2 µm PVDF filter (Thermo Fisher Scientific Inc., USA) in order to remove any larger aggregates or bacteria. Next, the FhuA concentration was determined by measuring the protein absorption at 280 nm using the UV–vis spectrophotometer SPECORD 210 (Analytik Jena AG, Germany). If needed, the FhuA solution was diluted to a concentration of 1 mg mL^{-1}. Controlled protein refolding was achieved by dialyzing the protein solution against MPD buffer (1:200) three times for 24 h at 4 °C using a dialysis membrane with a molecular weight cut-off (MWCO) of 12–14 kDa (Sigma-Aldrich, USA). Before the use in any experiment, the FhuA concentration was adjusted by dilution in MPD buffer and the concentration determined by UV–vis spectroscopy.

Langmuir Trough and Membrane Formation: Langmuir experiments were performed on a KSV Nima minitrough system equipped with two symmetrically movable barriers, 273 cm^2 surface area and a volume of 176 mL. Barrier movement was controlled by a servo controlled DCmotor and surface pressure was recorded using a platinum Wilhelmy plate (Biolin Scientific, Sweden) attached to a microelectronic feedback system (dynamic range = 0–250 mN m^{-1}, resolution 4 µN m^{-1}). Membrane formation and transfer to support materials was performed as follows. First, the Langmuir trough was thoroughly cleaned with ethanol, rinsed with Millipore pure water, and filled with phosphate buffer. Subsequently, the barriers of the Langmuir trough were fully closed, adsorbed particles were sucked away from the air–water interface and the phosphate buffer was refilled from behind the barriers. This procedure was repeated until the measured rise in surface pressure of the clean air–water interface upon full barrier compression was less than or equal to 0.05 mN m^{-1}. In a typical membrane fabrication experiment, 50 µL FhuA solution (FhuA in MPD buffer at a concentration of 6.3×10^{-6} M) was spread to the clean air–water interface in 25 µL aliquots. After 2 h of equilibration, the barriers of the Langmuir trough were set to motion at a speed of 1 mm min^{-1} to compress the adsorbed FhuA monolayer up to a surface pressure of 25 mN m^{-1}. While keeping the surface pressure constant, 1.76 mL glutaraldehyde solution (50 wt% in H_2O, Sigma-Aldrich, USA) was injected to the phosphate buffer subphase from behind the Langmuir trough barriers. Crosslinking proceeded for at least 2 h until the FhuA membrane was transferred to the respective substrate following the Langmuir–Schaefer method. Before drying in air, transferred FhuA membranes were washed in an MPD solution (5 vol% MPD in Millipore pure water) by dipping three times.

Substrates: QUANTIFOIL Multi A TEM girds equipped with a holey carbon film and hole dimensions ranging from 1 to 8 µm (Figure 2e; Figure S11, Supporting Information) and QUANTIFOIL R3/3 300-mesh holey carbon grids with 2 nm carbon support film (Figure S12, Supporting Information) were purchased from Quantifoil Micro Tools GmbH, Germany. Silicon nitride membrane windows with a single hole of 1 µm (thickness of silicon nitride membrane 100 nm) or 5 µm (thickness of silicon nitride membrane 500 nm) diameter for ion conductivity and water permeation measurements, respectively, were purchased from Silson Ltd, UK. The silicon substrates (100) were purchased from Entegris Inc., USA. Sintered aluminum oxide microfiltration membranes with a pore size of about 70 nm were obtained from Fraunhofer IKTS, Germany.

BAM: BAM images were acquired using an Accurion nanofilm_ultrabam with a field of view of 800 × 430 µm and a lateral resolution down to 2 µm. BAM was performed on a Kibron MicroTrough XL equipped with two symmetrically movable barriers, a surface area of 232 cm^2 and a volume of 145 mL. Surface pressure was recorded using a small diameter (0.51 mm) special alloy wire attached to a microelectronic feedback system (dynamic range = 0–130 mN m^{-1}, resolution 10 µN m^{-1}).

SFG: A Langmuir trough was filled with 80 mL of the phosphate buffer applied for membrane fabrication mentioned above dissolved in D_2O, before 6 nmol of the protein was carefully spread onto its surface. By precisely controlling the surface area using surface pressure as a feedback in real time, a surface pressure of 25 mN m^{-1} was achieved and retained in automatic compression mode (Kibron FilmwareX) throughout the experiment. The principles of the SFG technique have been introduced in detail elsewhere.[45] Briefly, an infrared laser beam in resonance with a molecular vibration, in this case the O–H stretch vibration, is overlapped in space and time with a visible laser beam. At the interface, the sum-frequency light of the two incoming beams is generated. Due to SFG selection rules, the generation of sum-frequency signals is forbidden in centrosymmetric media. The appearance of an SFG signal thus means that the molecules are preferentially aligned, breaking centrosymmetry. The SFG signal is enhanced at resonance with the molecular vibration. In the setup, the frequency range of interest was set mostly around the amide region, from which the secondary structure of the interfacial protein could be inferred. The measurements were taken both before and after 0.8 mL of the crosslinker and 50 wt% glutaraldehyde solution was added to the subphase. As a useful complement, calculated spectra based on a referenced protein database were also generated with a given angle of the protein's backbone to the surface normal, and a certain angular distribution, assumed to be Gaussian.

AFM: The AFM images were acquired in tapping mode with a Bruker Dimension Icon AFM equipped with OTESPA R3 tips (k= 26 N m^{-1}, f_0 = 300 kHz), when membranes were measured dry. PeakForce QNM was done in liquid using ScanAsyst Fluid tips (k = 0.7 N m^{-1}, f_0 = 150 kHz) with a peak force of 2 nN. Nanoscope (Version 9.1) and Nanoscope Analysis (Version 1.9) software were used for measurements and image processing, respectively. The Young's modulus E (Pa) of the FhuA ΔCVF^{tev} membrane measured in PeakForce QNM (Figure 3; Figure S14, Supporting Information) was estimated using a model deduced from point force elastic theory for homogenous membranes by Mueggenburg et al. as stated in Equation (1)[47–49]

$$E = \frac{3FR^2}{\pi h \delta^3} \quad (1)$$

where F is a point force applied to the center of the freestanding membrane (N), R is the radius of the hole covered by the membrane (m), h is the membrane thickness (m), and δ is the membrane deformation in the hole center (m). For calculation of the Young's modulus of the FhuA ΔCVF^{tev} membrane, the model was filled with the following data as measured in PeakForce QNM (Figure 3): F = 2 nN, R = 2.5 µm, h = 5 nm, and δ = 40 nm.

TEM: TEM images were acquired with a Thermo Fisher Talos F200C microscope (USA) at 200 kV at 57k× or 150k× magnification using a 4k × 4k Ceta 16M CMOS camera and the image acquisition software Velox 2.14. Plunge freezing of freshly transferred membranes into liquid ethane was done using a Leica EM GP2 plunge freezer after 5 s dual blotting at 10 °C and 90% humidity.

HIM: HIM images were acquired with a Carl Zeiss ORION Plus helium ion microscope (Germany) either in the standard secondary electron detection mode (Figure S17a, Supporting Information) or by employing a scanning transmission ion microscopy detector (dark-field: Figure 2e; Figure S17b, Supporting Information; bright-field: Figure S18a, Supporting Information).[59]

ThioGlo1 Labeling and Fluorescence Microscopy: A FhuA ΔCVF^{tev} monolayer membrane transferred to a silicon substrate was labeled with the thiol-reactive fluorescent dye ThioGlo1 according to a protocol established elsewhere.[22,58] Briefly, a 1.5 × 10^{-3} M stock solution of ThioGlo1 in acetonitrile was prepared and diluted in phosphate buffer to a concentration of 15 × 10^{-6} M. This solution was used to incubate the FhuA ΔCVF^{tev} membrane on top of the silicon substrate for 1 h, protected from light. After incubation, samples were washed by dipping three times into fresh Millipore pure water, dried in air, and investigated using fluorescence microscopy. The fluorescence microscopy images were acquired with a Leica DMi8 inverted fluorescence microscope (Leica Microsystems GmbH, Germany). Images were processed using Leica's LAS X software (Version 2.0.0).

Mass Loss Experiments: Water permeation through FhuA WT membranes was studied with mass loss measurements.[50] Silicon nitride membrane windows with 5 µm sized holes were used to prepare freestanding FhuA membranes. The FhuA membrane-coated chip was glued to a container cap, which in return was screwed on top of a container filled with 400 µL of Millipore pure water. The experiments started around 15 h later to make sure that the relative humidity inside the container reaches 100% and a steady-state of the mass change was reached. To confirm the reliability of the setup, a control measurement was first done with different-sized open apertures, as published here.[7] The container was placed into an enclosed oven with a constant temperature (30 ± 0.1) °C, and the RH inside the oven was controlled around 13% ± 2% by saturated LiCl solution.[60] Due to the water vapor pressure difference inside and outside the container, water evaporates in the container and then permeates the FhuA membrane. The mass loss of the container was measured after eight days by using a microbalance (Sartorius ME36S with a sensitivity of 1 µg). The water permeance P of the FhuA WT membrane was calculated by Equation (2)

$$P = \frac{\Delta m / M}{A t \Delta p} \quad (2)$$

where Δm is the mass change of the container (g), M is the molecular mass (g mol^{-1}), A is the membrane area (m^2), t is the time interval for an experiment (s), and Δp is the vapor pressure difference (Pa). In this study, Δp was around 3700 Pa.

Ion Conductivity Measurements: The ion conductivity measurements were performed using a specially designed microfluidic device made of two PMMA blocks. Each block contains a reservoir with a narrow channel for the electrolyte solution (the assembly of both reservoirs holds a volume of 250 µL). The end of each channel contains an embedded window in the size of the used silicon nitride membrane window to ensure precise placement of the sample. This device was already used to measure conductivity changes of thermoresponsive membranes and is well suited to detect small changes in resistance.[61,62] For preparation, both blocks were immersed into a phosphate buffer solution (10 × 10^{-3} M NaCl, 10 × 10^{-3} M sodium phosphate (NaPi), pH = 7) to exclude bubble formation in the measuring channel while filling the reservoirs. The silicon nitride membrane window coated with the respective membrane and a PDMS seal were placed in the intended position and the two blocks were joined by screws.

The electrical contact between the reservoirs was accomplished by two Ag/AgCl electrodes. In order to exclude external interferences, the measurements were performed in a Faraday cage at room temperature. For each sample, voltages in a range from ±1 to ± 20 mV were applied, and the current was measured with a time resolution of 1 kHz using an Axopatch 200B Amplifier (Molecular Devices, Biberach, Germany).

BSA Rejection Experiments: BSA rejection of FhuA membranes transferred to ceramic membrane supports (Fraunhofer IKTS, Germany) was measured using the set-up of a syringe pump (KDS 200/200P Legacy Syringe Pump, KD Scientific Inc., USA) described in Figure S20 of the Supporting Information. FhuA membrane coated supports were placed into Swinnex filter holders (Merck Millipore, USA) and filtration of a BSA solution (≈0.5 mg mL^{-1}) was performed at a flow rate of 0.1 mL min^{-1}. BSA concentration in feed, permeate, and retentate was determined by measuring the protein absorption at 280 nm using the UV–vis spectrophotometer SPECORD 210 (Analytik Jena AG, Germany).

Supporting Information

Supporting Information is available from the Wiley Online Library or from the author.

Acknowledgements

The Bundesministerium für Bildung und Forschung (BMBF) is kindly acknowledged for financial support in the framework of the BMBF-Forschertandem "Chiral Membranes II" (Förderkennzeichen: 031B0559). Work related to TEM measurements was funded by the Deutsche Forschungsgemeinschaft (DFG, German Research Foundation) under Germany's Excellence Strategy – EXC 2008 – 390540038 – UniSysCat. Further, the authors thank Synchrotron SOLEIL for beamtime. The authors acknowledge Nicolas Aubert and Dr. Philippe Fontaine for their excellent support at the SIRIUS beamline at the Synchrotron SOLEIL, France. The authors thank Prof. Dieter Hofmann and Prof. Dietmar Werner Auhl for valuable discussions as well as Aleksei Chumakov and Prof. Svetlana Santer for kind assistance with BAM experiments.

Open access funding enabled and organized by Projekt DEAL.

Conflict of Interest

The authors declare no conflict of interest.

Data Availability Statement

The data that support the findings of this study are available from the corresponding author upon reasonable request.

Keywords

glutaraldehyde, ion permeability, Langmuir technique, transmembrane proteins, ultrathin membranes, water permeance

Received: May 23, 2021
Revised: July 26, 2021
Published online: October 12, 2021

[1] S. Hube, M. Eskafi, K. F. Hrafnkelsdóttir, B. Bjarnadóttir, M. Á. Bjarnadóttir, S. Axelsdóttir, B. Wu, *Sci. Total Environ.* **2020**, *710*, 136375.
[2] M. Qasim, M. Badrelzaman, N. N. Darwish, N. A. Darwish, N. Hilal, *Desalination* **2019**, *459*, 59.
[3] M. Radjabian, V. Abetz, *Prog. Polym. Sci.* **2020**, *102*, 101219.
[4] R. W. Baker, *Membrane Technology and Applications*, Wiley, Chichester, UK **2012**.
[5] K. Celebi, J. Buchheim, R. M. Wyss, A. Droudian, P. Gasser, I. Shorubalko, J.-I. Kye, C. Lee, H. G. Park, *Science* **2014**, *344*, 289.
[6] F. Fornasiero, H. G. Park, J. K. Holt, M. Stadermann, C. P. Grigoropoulos, A. Noy, O. Bakajin, *Proc. Natl. Acad. Sci. USA* **2008**, *105*, 17250.
[7] Y. Yang, P. Dementyev, N. Biere, D. Emmrich, P. Stohmann, R. Korzetz, X. Zhang, A. Beyer, S. Koch, D. Anselmetti, A. Gölzhäuser, *ACS Nano* **2018**, *12*, 4695.
[8] Y. Yang, R. Hillmann, Y. Qi, R. Korzetz, N. Biere, D. Emmrich, M. Westphal, B. Büker, A. Hütten, A. Beyer, D. Anselmetti, A. Gölzhäuser, *Adv. Mater.* **2020**, *32*, 1907850.
[9] Z. Zhang, M. M. Rahman, C. Abetz, A.-L. Höhme, E. Sperling, V. Abetz, *Adv. Mater.* **2020**, *32*, 1907014.
[10] H. Ryu, A. Fuwad, S. Yoon, H. Jang, J. C. Lee, S. M. Kim, T.-J. Jeon, *Int. J. Mol. Sci.* **2019**, *20*, 1437.
[11] A. A. Vorobieva, P. White, B. Liang, J. E. Horne, A. K. Bera, C. M. Chow, S. Gerben, S. Marx, A. Kang, A. Q. Stiving, S. R. Harvey, D. C. Marx, G. N. Khan, K. G. Fleming, V. H. Wysocki, D. J. Brockwell, L. K. Tamm, S. E. Radford, D. Baker, *Science* **2021**, *371*, eabc8182.
[12] T. Mirzaei Garakani, D. F. Sauer, M. A. S. Mertens, J. Lazar, J. Gehrmann, M. Arlt, J. Schiffels, U. Schnakenberg, J. Okuda, U. Schwaneberg, *ACS Catal.* **2020**, *10*, 10946.
[13] H. Killmann, R. Benz, V. Braun, *EMBO J.* **1993**, *12*, 3007.
[14] D. Wong, T.-J. Jeon, J. Schmidt, *Nanotechnology* **2006**, *17*, 3710.
[15] M. Kumar, M. Grzelakowski, J. Zilles, M. Clark, W. Meier, *Proc. Natl. Acad. Sci. USA* **2007**, *104*, 20719.
[16] P. S. Zhong, T. Chung, K. Jeyaseelan, A. Armugam, *J. Membr. Sci.* **2012**, *407–408*, 27.
[17] C. Edlinger, T. Einfalt, M. Spulber, A. Car, W. Meier, C. G. Palivan, *Nano Lett.* **2017**, *17*, 5790.
[18] M. Kumar, J. E. O. Habel, Y.-X. Shen, W. P. Meier, T. Walz, *J. Am. Chem. Soc.* **2012**, *134*, 18631.
[19] S. S. Klara, P. O. Saboe, I. T. Sines, M. Babaei, P.-L. Chiu, R. DeZorzi, K. Dayal, T. Walz, M. Kumar, M. S. Mauter, *J. Am. Chem. Soc.* **2016**, *138*, 28.
[20] Y.-M. Tu, W. Song, T. Ren, Y.-X. Shen, R. Chowdhury, P. Rajapaksha, T. E. Culp, L. Samineni, C. Lang, A. Thokkadam, D. Carson, Y. Dai, A. Mukthar, M. Zhang, A. Parshin, J. N. Sloand, S. H. Medina, M. Grzelakowski, D. Bhattacharya, W. A. Phillip, E. D. Gomez, R. J. Hickey, Y. Wei, M. Kumar, *Nat. Mater.* **2020**, *19*, 347.
[21] H. Wang, T.-S. Chung, Y. W. Tong, K. Jeyaseelan, A. Armugam, Z. Chen, M. Hong, W. Meier, *Small* **2012**, *8*, 1185.
[22] T. Mirzaei Garakani, Z. Liu, U. Glebe, J. Gehrmann, J. Lazar, M. A. S. Mertens, M. Möller, N. Hamzelui, L. Zhu, U. Schnakenberg, A. Böker, U. Schwaneberg, *ACS Appl. Mater. Interfaces* **2019**, *11*, 29276.
[23] P. H. H. Duong, T.-S. Chung, K. Jeyaseelan, A. Armugam, Z. Chen, J. Yang, M. Hong, *J. Membr. Sci.* **2012**, *409–410*, 34.
[24] Y. Li, S. Qi, M. Tian, W. Widjajanti, R. Wang, *Desalination* **2019**, *467*, 103.
[25] K. Altintoprak, A. Seidenstücker, P. Krolla-Sidenstein, A. Plettl, H. Jeske, H. Gliemann, C. Wege, *Bioinspired, Biomimetic Nanobiomater.* **2017**, *6*, 208.
[26] K. Altintoprak, F. Farajollahi, A. Seidenstücker, T. Ullrich, N. L. Wenz, P. Krolla, A. Plettl, P. Ziemann, O. Marti, P. Walther, D. Exner, R. Schwaiger, H. Gliemann, C. Wege, *Bioinspired, Biomimetic Nanobiomater.* **2019**, *8*, 47.
[27] S. Zhang, J. Zhang, W. Fang, Y. Zhang, Q. Wang, J. Jin, *Nano Lett.* **2018**, *18*, 6563.
[28] N. C. Mougin, P. van Rijn, H. Park, A. H. E. Müller, A. Böker, *Adv. Funct. Mater.* **2011**, *21*, 2470.
[29] P. van Rijn, N. C. Mougin, D. Franke, H. Park, A. Böker, *Chem. Commun.* **2011**, *47*, 8376.
[30] P. van Rijn, N. C. Mougin, A. Böker, *Polymer* **2012**, *53*, 6045.
[31] P. van Rijn, H. Park, K. Özlem Nazli, N. C. Mougin, A. Böker, *Langmuir* **2013**, *29*, 276.
[32] P. van Rijn, M. Tutus, C. Kathrein, N. C. Mougin, H. Park, C. Hein, M. P. Schürings, A. Böker, *Adv. Funct. Mater.* **2014**, *24*, 6762.
[33] H. Charan, J. Kinzel, U. Glebe, D. Anand, T. M. Garakani, L. Zhu, M. Bocola, U. Schwaneberg, A. Böker, *Biomaterials* **2016**, *107*, 115.
[34] H. Charan, U. Glebe, D. Anand, J. Kinzel, L. Zhu, M. Bocola, T. M. Garakani, U. Schwaneberg, A. Böker, *Soft Matter* **2017**, *13*, 2866.
[35] O. Barbosa, C. Ortiz, Á. Berenguer-Murcia, R. Torres, R. C. Rodrigues, R. Fernandez-Lafuente, *RSC Adv.* **2014**, *4*, 1583.
[36] G. T. Hermanson, *Bioconjugate Techniques*, Elsevier, Amsterdam **2013**.
[37] D. R. Walt, V. I. Agayn, *Trends Anal. Chem.* **1994**, *13*, 425.
[38] Z. Liu, I. Ghai, M. Winterhalter, U. Schwaneberg, *ACS Sens.* **2017**, *2*, 1619.
[39] M. Krewinkel, T. Dworeck, M. Fioroni, *J. Nanobiotechnol.* **2011**, *9*, 33.
[40] I. Langmuir, V. J. Schaefer, *J. Am. Chem. Soc.* **1938**, *60*, 1351.
[41] K. Mladenova, S. D. Petrova, T. D. Andreeva, V. Moskova-Doumanova, T. Topouzova-Hristova, Y. Kalvachev, K. Balashev, S. S. Bhattacharya, C. Chakarova, Z. Lalchev, J. A. Doumanov, *Colloids Surf., B* **2017**, *149*, 226.
[42] T. D. Andreeva, S. D. Petrova, K. Mladenova, V. Moskova-Doumanova, T. Topouzova-Hristova, Y. Petseva, N. Mladenov, K. Balashev, Z. Lalchev, J. A. Doumanov, *Colloids Surf., B* **2018**, *161*, 192.
[43] G. Gonzalez, F. MacRitchie, *J. Colloid Interface Sci.* **1970**, *32*, 55.
[44] D. J. Adams, M. T. A. Evans, J. R. Mitchell, M. C. Phillips, P. M. Rees, *J. Polym. Sci., Part C: Polym. Symp.* **1971**, *34*, 167.
[45] S. Hosseinpour, S. J. Roeters, M. Bonn, W. Peukert, S. Woutersen, T. Weidner, *Chem. Rev.* **2020**, *120*, 3420.
[46] B. Pittenger, N. Erina, C. Su, in *Nanomechanical Analysis of High Performance Materials*, Vol. *203* (Ed: A. Tiwari), Springer, Dordrecht, The Netherlands **2014**, p. 31.
[47] K. E. Mueggenburg, X.-M. Lin, R. H. Goldsmith, H. M. Jaeger, *Nat. Mater.* **2007**, *6*, 656.
[48] U. Komaragiri, M. R. Begley, J. G. Simmonds, *J. Appl. Mech.* **2005**, *72*, 203.
[49] K.-T. Wan, S. Guo, D. A. Dillard, *Thin Solid Films* **2003**, *425*, 150.
[50] ASTM E96/E96m-16, Standard Test Methods for Water Vapor Transmission of Materials, ASTM International, West Conshohocken, PA **2016**.
[51] J. D. Faraldo-Gómez, G. R. Smith, M. S. P. Sansom, *Biophys. J.* **2003**, *85*, 1406.
[52] D. Some, H. Amartely, A. Tsadok, M. Lebendiker, *J. Visualized Exp.* **2019**.

[53] D. Anand, G. V. Dhoke, J. Gehrmann, T. M. Garakani, M. D. Davari, M. Bocola, L. Zhu, U. Schwaneberg, *Chem. Commun.* **2019**, *55*, 5431.
[54] X. Guan, L.-Q. Gu, S. Cheley, O. Braha, H. Bayley, *ChemBioChem* **2005**, *6*, 1875.
[55] F. Haque, J. Lunn, H. Fang, D. Smithrud, P. Guo, *ACS Nano* **2012**, *6*, 3251.
[56] J. Kinzel, D. F. Sauer, M. Bocola, M. Arlt, T. Mirzaei Garakani, A. Thiel, K. Beckerle, T. Polen, J. Okuda, U. Schwaneberg, *Beilstein J. Org. Chem.* **2017**, *13*, 1498.
[57] C. Michaux, N. C. Pomroy, G. G. Privé, *J. Mol. Biol.* **2008**, *375*, 1477.
[58] F. Philippart, M. Arlt, S. Gotzen, S.-J. Tenne, M. Bocola, H.-H. Chen, L. Zhu, U. Schwaneberg, J. Okuda, *Chemistry* **2013**, *19*, 13865.
[59] D. Emmrich, A. Wolff, N. Meyerbröker, J. K. N. Lindner, A. Beyer, A. Gölzhäuser, *Beilstein J. Nanotechnol.* **2021**, *12*, 222.
[60] L. Greenspan, *J. Res. Natl. Bur. Stand., Sec. A* **1977**, *81A*, 89.
[61] J. Bookhold, M. Dirksen, L. Wiehemeier, S. Knust, D. Anselmetti, F. Paneff, X. Zhang, A. Gölzhäuser, T. Kottke, T. Hellweg, *Soft Matter* **2021**, *17*, 2205.
[62] M. Dirksen, T. Brändel, S. Großkopf, S. Knust, J. Bookhold, D. Anselmetti, T. Hellweg, *RSC Adv.* **2021**, *11*, 22014.